Two Adaptive Sliding Mode Control Algorithms for Vehicle Stability Enhancement

*Anh-Tuan Le**

Faculty of Electrical and Electronics Engineering, Ton Duc Thang University, Ho Chi Minh City, Vietnam.

*Corresponding Author:Anh-Tuan Le (email:leanhtuan1@tdtu.edu.vn)
(Received: 29-March-2024; accepted: 12-September-2024; published: 30-September-2024)
http://dx.doi.org/10.55579/jaec.202483.458

Abstract. *This paper discusses two adaptive sliding mode control (ASMC) algorithms for enhancing vehicle stability through direct yaw moment control (DYC). DYC is based on a logic process derived from the understeering and oversteering behavior of a cornering vehicle. Furthermore, to achieve DYC in a four-wheeled passenger vehicle, the reference yaw moment computed by the proposed algorihms is converted into a braking pressure that is to be applied to the four wheels. The objective is to minimize the yaw rate error and constrain the sideslip angle to an acceptable range. According to Lyapunov theory, complete stability analysis guarantees the closed-loop stability and robustness of a control system. Simulation results were used to compare the two ASMC algorithms, and both algorithms showed high performance even under critical operating conditions.*

Keywords: *Adaptive sliding mode control (ASMC) algorithm, direct yaw moment control (DYC), Lyapunov theory, vehicle stability.*

1. Introduction

Recently, driving safety in passenger vehicles has been considerably improved. It is considered a key aspect in the design of a vehicle. Active safety systems are known by different denominations, namely electronic stability control, electronic stability program, dynamic stability control, vehicle stability control (VSC), and vehicle dynamic control systems.

Driving safety systems facilitate effective driver control on curves and slippery roads by actively constraining the oversteering or understeering behavior of a vehicle (Fig. 1), thereby reducing the risk of fatal crashes substantially. In particular, during cornering, the control of the yaw rate and vehicle sideslip angle helps maintain vehicle stability. Numerous studies have obtained impoved vehicle response by either controlling the yaw rate [1–5] or accurately estimating the vehicle sideslip angle [6–10]. Both of these variables should be controlled for achieving the desired vehicle response. In recent years, VSC systems have been designed for controlling both variables to follow their reference values [11–14]. Studies [11–21] have demonstrated the effectiveness of direct yaw moment control (DYC) in enhancing vehicle control and stability. DYC involves the conversion of yaw moment into braking pressure [11–13, 15] or braking torque [14, 16–21], which is then applied to the wheels. Recently, active safety systems for electric vehicles whose motors are connected to each wheel separately have received considerable interest [1–7, 14, 16–21]. By contrast, only a few studies have been conducted

on the application of VSC systems to internal combustion engine vehicles or hydraulic-model-based electric vehicles [11–13, 15]. In practice, an unstable vehicle tends to rapidly spin or bounce out of the desired trajectory, and even a short delay in achieving VSC can result in fatal accidents. Therefore, electric vehicles with wheel motors are easier to control than internal-combustion engine vehicles, which exhibit delays associated with brake hydraulics and response to braking [18]. Thus far, fuzzy control, model predictive control, adaptive control, sliding mode control (SMC), internal model control, optimal control, and a game theory approach have been considered the best choices for controlling VSC systems; neural networks and hidden Markov models can also be used for the purpose [1–5], [10–23]. My previous study described the specific advantages and disadvantages of each control method [11].

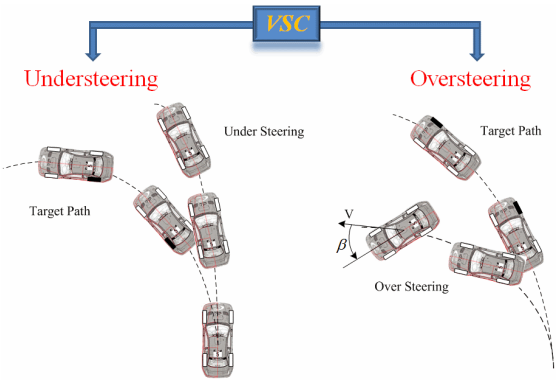

Fig. 1: Understeering and oversteering behavior.

SMC has attracted considerable attention in VSC applications. Its notable features include robustness, fast convergence, simple implementation, and insensitivity to vehicle parameter fluctuations and uncertainties. Owing to these advantages, SMC has been successfully applied to VSC systems [14]. In this paper, three parameter adaptation laws are added to the control law to eliminate uncertainties in the system caused by model inaccuracies and disturbances. Moreover, the combination of adaptive and sliding mode theories for designing a VSC system with the ASMC of two variables yaw rate and vehicle sideslip angle is considered. In my previous study [11], a sliding function used for designing an ASMC algorithm which was named the first ASMC in this study was a weighted combination of the yaw rate and sideslip angle errors as follows:

$$S_1 = e_\gamma + \xi e_\beta \tag{1}$$

In [11], the first ASMC law derived using the sliding function in Eq. 1 ensures that the phase trajectory of the system reach and remain at the sliding surface $S_1 = 0$, provided the yaw rate and sideslip angle errors have the same sign. These two errors are guaranteed to be canceled out in Eq. 1. However, the signs of the errors may vary with changing road and driving conditions on the vehicle wheels. Consequently, although the system trajectory may approach and reach the sliding surface in a finite time, the errors are not guaranteed to be canceled out. Therefore, the following approach involving an improved sliding function is proposed

$$S_2 = |e_\gamma| + \xi\,|e_\beta| \tag{2}$$

The present paper proposes an ASMC law impoved using the sliding function in Eq. 2 that can overcome the aforementioned disadvantages, namely the second ASMC algorithm. The approach involving an improved sliding function can be used to make the phase trajectory of the system reach and remain at the sliding surface $S_2 = 0$, regardless of changes in the road and driving conditions. Both ASMC algorithms require accurate information regarding the steering angle, longitudinal velocity, yaw rate, vehicle sideslip angle, and tire slip angle to generate a stabilizing yaw moment. In practice, the longitudinal velocity can be determined from the wheel speed, and the steering angle, yaw rate, and wheel speed can be determined using widely available and inexpensive sensors. Furthermore, the vehicle sideslip angle and tire slip angle can be determined if the lateral tire forces and vehicle velocity are known, respectively. My previous study [24] provided a detailed discussion of the estimation methods for vehicle variables that cannot be measured. A major feature of this study is the discussion of positive effects of the ASMC algorithms mentioned in simulation result section. To verify the performace of controllers that are proposed in the current study, for simplicity, the required information on the

aforementioned vehicle variables was obtained from a CarSim vehicle model.

The contribution of this study is the presentation of a DYC system that involves a combination of adaptive and SMC; this system can enhance vehicle stability under extremely critical driving conditions, namely normal and high speeds on road surfaces with high, moderate, very low, and variable friction coefficients. A comparison with a proposed controller involving only SMC [14] showed that the controller proposed in the previous study exhibits high performance for an electric vehicle with a low speed on roads with a high friction coefficient (dry roads). However, whether the yaw rate and sideslip angle responses remain stable when the vehicle is driven under critical conditions such as at high speeds and on roads with an extremely low or variable friction coefficient (icy roads or variations from dry road conditions to icy road conditions) remains unresolved. In general, both approaches (based on different ASMC algorithms) presented in this study are effective in achieving vehicle control. However, the second approach is superior, especially during extremely critical driving maneuvers. In this study, the direct yaw moment was generated by applying forces to all wheels of a four-wheeled vehicle, contrast to a previous study that applied forces only to the two rear wheels [14]. Therefore, under critical condition, because of the yaw moment generated from the application of forces to the four wheels, the vehicle is more stable when the controller is activated.

This paper proposes a DYC system that involves a combination of two ASMC algorithms and a control logic process for solving the stability problem associated with the yaw rate and vehicle sideslip angle. The algorithms were applied to a CarSim vehicle model with an internal combustion engine, and the dynamics of the model were controlled using the braking pressure on the four wheels as vehicle inputs. On the basis of the Lyapunov theory, the stability and robustness of the control system using the second ASMC algorithm were found to be such that the system trajectory approached the sliding surface. Generally, control is achieved by generating pressure for the active braking of the four vehicle wheels to stabilize the vehicle yaw rate and narrow sideslip angle for different driving maneuvers. The proposed system ensures a narrow yaw-rate error and a sideslip angle in an acceptable range. In a previous study [9], the desired range of the sideslip angle was approximately $\pm 2^0$, and in some critical driving conditions, it can be allowed to be in an approximate range of $\pm 5^0$ or a maximum range of $\pm 12^0$ [8, 9, 13, 25]. In the current study, DYC was achieved using a reference pressure generator and a hydraulic pressure control. The proposed DYC system converts the reference yaw moment computed by the two ASMC algorithms into the braking pressure that is to be applied to the four wheels. Therefore, the controller could generate larger yaw moments in critical situations. Compared with a previous study [15], the control logic process for generating reference pressure was improved by applying more pressure to the four wheels, thus increasing the compensated yaw moment when the steering angle began to change to zero. This process yielded a faster yaw-rate response and a smaller steady-state error in the yaw rate.

The rest of this paper is organized as follows: Vehicle models used for developing the proposed VSC system and deriving the proposed algorithms are described in Section 2. . Section 3. introduces the proposed VSC system that involves two ASMC algorithms, and Section 4. presents and discusses simulation results. Finally, the conclusions are outlined in Section 5. .

2. Vehicle models

2.1. CarSim model

A high-order model, CarSim, was considered for control use. The model describes the overall motion of a full vehicle model, namely direction, speed control, and external conditions such as road information and drag, and it was therefore considered to be appropriate for vehicle handling simulations. CarSim is commercial software exhibiting a well-defined user interface, and it is widely used as simulation software in the automotive industry. In addition, CarSim had already been validated, thus rendering it appropri-

ate for the simulation of the dynamics of a real vehicle. In this study, CarSim software was used for evaluating the performance of the proposed controllers. The CarSim vehicle configuration is presented in Fig. 2.

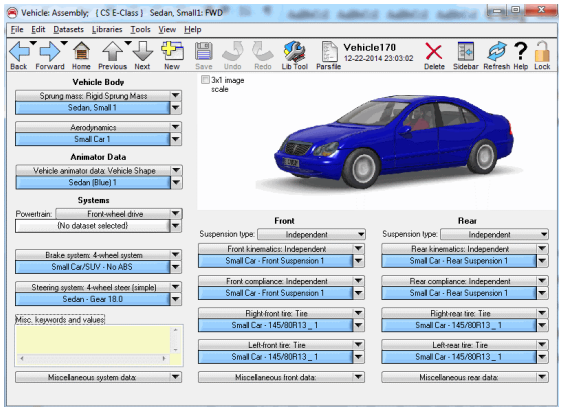

Fig. 2: Vehicle configuration of CarSim [26].

2.2. Seven-degree-of-freedom vehicle model

The model used for designing the controller in this study was a simplified model with seven degrees of freedom (7-DOF), corresponding to the longitudinal and lateral velocities (V_x and V_y), yaw rate (γ), and the rotational speeds of the four wheels (ω_i). The following equations of motion for the 7-DOF model were derived from Fig. 3 by applying the Newton-Euler approach to the wheels and vehicle. Besides, details on the description of variables and parameters in the model used for the control system are shown in Table 1 below. Longitudinal motion

$$\dot{V}_x = \frac{1}{m}\begin{pmatrix} m\gamma V_y + F_{x1}\cos\delta_l + F_{x2}\cos\delta_r + \ldots \\ F_{x3} + F_{x4} - F_{y1}\sin\delta_l - F_{y2}\sin\delta_r \end{pmatrix} \tag{3}$$

Lateral motion

$$\dot{V}_y = \frac{1}{m}\begin{pmatrix} -m\gamma V_x + F_{x1}\sin\delta_l + F_{x2}\sin\delta_r + \ldots \\ F_{y3} + F_{y4} + F_{y1}\cos\delta_l + F_{y2}\cos\delta_r \end{pmatrix} \tag{4}$$

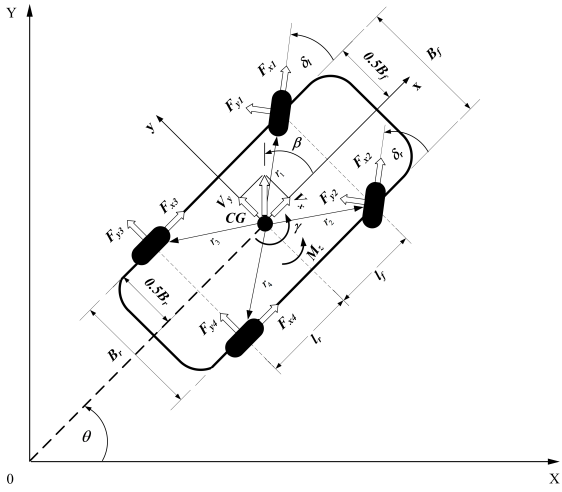

Fig. 3: The 7-DOF vehicle model.

Tab. 1: Nomenclature.

Variables and Parameters	Description
B_f	Front track width
B_r	Rear track width
C_i	Cornering stiffness of each wheel
F_{xi}	Longitudinal force on each wheel
F_{yi}	Lateral force on each wheel
I_z	Mass moment of inertia about the z-axis
l	Wheelbase
l_f	Distance from center of gravity (CG) to front axle
l_r	Distance from CG to rear axle
m	Vehicle mass
M_z	Yaw moment associated with differential Brakes
r	Wheel radius
V_x	Longitudinal velocity
V_y	Lateral velocity
α_i	Slip angle of each wheel
β	Vehicle side-slip angle
δ	Steering angle
δ_l	Steering angle of left front wheel
δ_r	Steering angle of right front wheel
δ_w	Steering wheel angle
γ	Yaw rate
μ	Frictional coefficient
θ	Vehicle heading angle measured from the x-axis
ω_n	Speed of the wheels

Yaw motion

$$\dot{\gamma} = \frac{1}{I_z}\begin{pmatrix} F_{y1}\left(l_f\cos\delta_l + 0.5B_f\sin\delta_l\right) - \ldots \\ \left(F_{y3} + F_{y4}\right)l_r + \ldots \\ F_{y2}\left(l_f\cos\delta_r - 0.5B_f\sin\delta_r\right) + \ldots \\ F_{x1}\left(-0.5B_f\cos\delta_l + l_f\sin\delta_l\right) + \ldots \\ F_{x2}\left(l_f\sin\delta_r + 0.5B_f\cos\delta_r\right) - \ldots \\ 0.5B_r\left(F_{x3} - F_{x4}\right) \end{pmatrix} \tag{5}$$

Rotational motion of the four wheels

$$\dot{\omega}_i = \frac{1}{I_w}\left(rF_{xi} - T_{bi}\right), \quad (i = 1, 4) \tag{6}$$

3. Control system design

3.1. System overview

The entire structural scheme of the control system that can be used for vehicle stability improvement is presented in Fig. 4. The global inputs of the control system comprise the steering wheel angle, longitudinal velocity, and feedback and reference values of the yaw rate and sideslip angle. The outputs are the controlled responses of the yaw rate and sideslip angle. The system comprises reference yaw rate and sideslip angle generators, ASMC algorithms for generating the desired yaw moment, a control-logic-based pressure generator for calculating the braking pressure to be applied to the wheels from the yaw moment according to the required vehicle yaw rate and sideslip angle, and a CarSim vehicle model for verifying the performance of the vehicle stability controllers.

3.2. First ASMC algorithm

The first ASMC algorithm was derived from the aforementioned 7-DOF vehicle model. This algorithm was used to generate a reasonably compensated yaw moment, which was required for determining the braking pressure that was to be applied to the vehicle wheels. The reader can refer to my previous paper [11] for a discussion on this algorithm.

3.3. Second ASMC algorithm

For deriving the second algorithm, the yaw rate was of primary concern since it was an essential variable for demonstrating vehicle stability. The second algorithm was designed under the assumption that $\delta_l \approx \delta_r \approx \delta$. Therefore, the yaw motion Eq. 5, becomes

$$\begin{aligned} I_z\dot{\gamma} = {} & l_f\left(F_{x1} + F_{x2}\right)\sin\delta + l_f\left(F_{y1} + F_{y2}\right)\cos\delta - \ldots \\ & l_r\left(F_{y3} + F_{y4}\right) + 0.5B_f\left(F_{x2} - F_{x1}\right)\cos\delta + \ldots \\ & 0.5B_r\left(F_{x4} - F_{x3}\right) + 0.5B_f\left(F_{y1} - F_{y2}\right)\sin\delta \end{aligned} \tag{7}$$

The steering angle of the front wheels is typically low. Therefore, supposing that the steering angle is low such that $\sin\delta \approx 0$ and $\cos\delta \approx 0$; Eq. 7 can be derived as

$$\begin{aligned} I_z\dot{\gamma} = {} & l_f\left(F_{y1} + F_{y2}\right) - l_r\left(F_{y3} + F_{y4}\right) + \ldots \\ & 0.5B_f\left(F_{x2} - F_{x1}\right) + 0.5B_r\left(F_{x4} - F_{x3}\right) \end{aligned} \tag{8}$$

The yaw moment resulting from the application of differential brakes was defined as

$$M_z = 0.5B_f\left(F_{x2} - F_{x1}\right) + 0.5B_r\left(F_{x4} - F_{x3}\right) \tag{9}$$

According to the theory of ground vehicles [27], the slip angles of the front and rear wheels can be calculated from the expressions

$$\alpha_f = \beta + \frac{\gamma l_f}{V_x} - \delta \tag{10}$$

$$\alpha_r = \beta - \frac{\gamma l_r}{V_x} \tag{11}$$

The lateral tire forces were assumed to be linear functions of the slip angles [27]. In addition, under the condition that the front slip angles almost precisely match each other and that the rear slip angles match to the same degree as the front slip angles, Eqs. 9 and 10 can be used to obtain the following expressions:

$$\begin{aligned} F_{y1} + F_{y2} &\approx -\alpha_f\left(C_1 + C_2\right) \\ &= -\left(C_1 + C_2\right)\left(\beta + \tfrac{\gamma l_f}{V_x} - \delta\right) \end{aligned} \tag{12}$$

$$\begin{aligned} F_{y3} + F_{y4} &\approx -\alpha_r\left(C_3 + C_4\right) \\ &= -\left(C_3 + C_4\right)\left(\beta - \tfrac{\gamma l_r}{V_x}\right) \end{aligned} \tag{13}$$

Substituting Eqs. 9, 12 and 13 into Eq. 8 yields

$$\begin{aligned} I_z\dot{\gamma} = {} & -\tfrac{\gamma}{V_x}\left(l_f^2\left(C_1 + C_2\right) + l_r^2\left(C_3 + C_4\right)\right) - \ldots \\ & \beta\left(l_f\left(C_1 + C_2\right) - l_r\left(C_3 + C_4\right)\right) + \ldots \\ & \delta l_f\left(C_1 + C_2\right) + M_z \end{aligned} \tag{14}$$

The following expressions is set:

$$\rho_1 = l_f^2\left(C_1 + C_2\right) + l_r^2\left(C_3 + C_4\right) \tag{15}$$

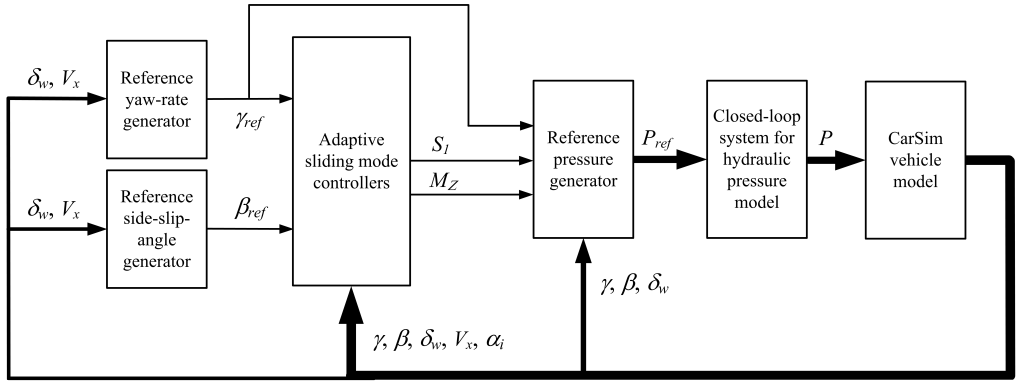

Fig. 4: Structural scheme of a vehicle stability control system.

$$\rho_2 = l_f\left(C_1 + C_2\right) - l_r\left(C_3 + C_4\right) \tag{16}$$

$$\rho_3 = l_f\left(C_1 + C_2\right) \tag{17}$$

Therefore, Eq. 14 becomes

$$\dot{\gamma} = \frac{1}{I_z}\left(-\frac{\gamma}{V_x}\rho_1 - \beta\rho_2 + \delta\rho_3 + M_z\right) \tag{18}$$

or

$$M_z = \frac{\gamma}{V_x}\rho_1 + \beta\rho_2 - \delta\rho_3 + I_z\dot{\gamma} \tag{19}$$

In my previous study [11], a control system was designed using the first ASMC algorithm; the algorithm involves a sliding function S_1 (1), which is a weighted combination of the yaw rate and sideslip angle errors. After the analysis and demonstration of the stability of the control system [11], the tracking error S1 of a closed-loop system was concluded to asymptotically converge to zero as the time approaches infinity. However, this conclusion is correct only if both the yaw rate and sideslip angle errors in Eq. 1 have the same sign. These errors are not guaranteed to converge to zero at $t \to \infty$ because their signs may change when the road and driving conditions are critical. To overcome this drawback, a second ASMC algorithm is proposed; the algorithm involves the use of a second sliding function S_2 (2), which is a weighted combination of the absolute values of the yaw rate and sideslip angle errors for analysis and control design. The sliding function in Eq. 2 is similar to

$$S_2 = \left|\gamma - \gamma_{ref}\right| + \xi\left|\beta - \beta_{ref}\right| \tag{20}$$

The time derivative of Eq. 2 or Eq. 20 is

$$\dot{S}_2 = \left(\dot{\gamma} - \dot{\gamma}_{ref}\right)\mathrm{sgn}\left(e_\gamma\right) + \xi\dot{e}_\beta\mathrm{sgn}\left(e_\beta\right) \tag{21}$$

Multiplying both sides of Eq. 21 by $\mathrm{sgn}\left(e_\gamma\right)$ and changing the result yields

$$\dot{\gamma} = \dot{\gamma}_{ref} + \dot{S}_2\mathrm{sgn}\left(e_\gamma\right) - \xi\dot{e}_\beta\mathrm{sgn}\left(e_\gamma e_\beta\right) \tag{22}$$

In the present study, the tracking error dynamics were defined as [28]

$$\dot{S}_2 = -K_pS_2 - K_s\mathrm{sgn}\left(S_2\right) \tag{23}$$

Hence, the control law derived from Eqs. 19, 22, and 23 is

$$\begin{aligned} M_z = {} & \tfrac{\gamma}{V_x}\rho_1 + \beta\rho_2 - \delta\rho_3 + \ldots \\ & I_z\left(\dot{\gamma}_{ref} - K_pS_2\mathrm{sgn}\left(e_\gamma\right) - \ldots\right. \\ & \left. K_s\mathrm{sgn}\left(S_2e_\gamma\right) - \xi\dot{e}_\beta\mathrm{sgn}\left(e_\gamma e_\beta\right)\right) \end{aligned} \tag{24}$$

If the phase trajectory of the system is to approach the sliding surface $S_2 = 0$ and remain there under model uncertainties, the control law must be determined. Therefore, a setting similar to that in Eq. 23 ensures that the designed control law in Eq. 24 satisfies the aforementioned control objective because the control law involves the following Lyapunov function:

$$V_1 = \frac{1}{2}{S_2}^2 \tag{25}$$

Taking the time derivative of Eq. 25 and then using Eq. 23 yield

$$\begin{aligned} \dot{V}_1 &= S_2\dot{S}_2 = S_2\left(-K_pS_2 - K_s\mathrm{sgn}\left(S_2\right)\right) \\ &= -K_pS_2^2 - K_s\left|S_2\right| \end{aligned} \tag{26}$$

Eq. 26 shows that $\dot{V}_1 \leq 0$. According to Lyapunov theory, the SMC law in Eq. 24 is stable, and for a closed-loop system, the tracking error

in Eq. 2 asymptotically converges to zero as the time approaches infinity.

Remark 1: In the design of nonlinear systems, ASMC is extremely effective for stabilizing uncertain systems, such as fast response, favorable transient performance, and robustness against disturbances or model uncertainties. Therefore, ASMC has the potential to stabilize complex non-linear systems such as VSC systems. In practice, $\rho_i\,(i=1,3)$ parameters in Eqs. 15-17 change with the vehicle load and road conditions. Hence, the SMC law in Eq. 24 can be rewritten as follows:

$$\begin{aligned} M_z = {} & \tfrac{\gamma}{V_x}\hat{\rho}_1 + \beta\hat{\rho}_2 - \delta\hat{\rho}_3 + \ldots \\ & I_z\left(\dot{\gamma}_{ref} - K_p S_2 \mathrm{sgn}\left(e_\gamma\right) - \ldots\right. \\ & \left. K_s \mathrm{sgn}\left(S_2 e_\gamma\right) - \xi \dot{e}_\beta \mathrm{sgn}\left(e_\gamma e_\beta\right)\right) \end{aligned} \tag{27}$$

where $\hat{\rho}_i$ is the estimated value of the unknown parameters $\rho_i\,(i=1,3)$. Let

$$\tilde{\rho}_i = \hat{\rho}_i - \rho_i, \quad (i=1,3) \tag{28}$$

Theorem: For vehicle yaw dynamics using the proposed sliding function S2, the modified control law in Eq. 27 ensures that the phase trajectory of the closed-loop system can be driven to the sliding surface $S_2 = 0$ as the time approaches infinity and that the phase trajectory can finally converge to a predefined reference trajectory under the model uncertainties.

Proof. The Lyapunov function candidate is defined as follows:

$$V_2 = \frac{1}{2}S_2^2 + \frac{1}{2K_1}\tilde{\rho}_1^2 + \frac{1}{2K_2}\tilde{\rho}_2^2 + \frac{1}{2K_3}\tilde{\rho}_3^2 \tag{29}$$

Differentiating Eq. 29 with respect to time yields

$$\dot{V}_2 = S_2\dot{S}_2 + \frac{1}{K_1}\tilde{\rho}_1\dot{\tilde{\rho}}_1 + \frac{1}{K_2}\tilde{\rho}_2\dot{\tilde{\rho}}_2 + \frac{1}{K_3}\tilde{\rho}_3\dot{\tilde{\rho}}_3 \tag{30}$$

Substituting Eq. 27 into Eq. 18, using Eq. 21, and then extracting from Eq. 28 yield

$$\begin{aligned} \dot{S}_2 = {} & \tfrac{\gamma \mathrm{sgn}(e_\gamma)}{I_z V_x}\tilde{\rho}_1 + \tfrac{\beta \mathrm{sgn}(e_\gamma)}{I_z}\tilde{\rho}_2 - \ldots \\ & \tfrac{\delta \mathrm{sgn}(e_\gamma)}{I_z}\tilde{\rho}_3 - K_p S_2 - K_s \mathrm{sgn}\left(S_2\right) \end{aligned} \tag{31}$$

Substituting Eq. 31 into Eq. 30 yields

$$\begin{aligned} \dot{V}_2 = {} & S_2\left(\tfrac{\gamma \mathrm{sgn}(e_\gamma)}{I_z V_x}\tilde{\rho}_1 + \tfrac{\beta \mathrm{sgn}(e_\gamma)}{I_z}\tilde{\rho}_2 - \ldots\right. \\ & \left.\tfrac{\delta \mathrm{sgn}(e_\gamma)}{I_z}\tilde{\rho}_3 - K_p S_2 - K_s \mathrm{sgn}\left(S_2\right)\right) \\ & + \tfrac{1}{K_1}\tilde{\rho}_1\dot{\tilde{\rho}}_1 + \tfrac{1}{K_2}\tilde{\rho}_2\dot{\tilde{\rho}}_2 + \tfrac{1}{K_3}\tilde{\rho}_3\dot{\tilde{\rho}}_3 \end{aligned} \tag{32}$$

The parameter adaptation laws are selected as follows:

$$\dot{\hat{\rho}}_1 = \dot{\tilde{\rho}}_1 = -\frac{K_1\gamma S_2 \mathrm{sgn}\left(e_\gamma\right)}{I_z V_x} - \sigma_1\tilde{\rho}_1 \tag{33}$$

$$\dot{\hat{\rho}}_2 = \dot{\tilde{\rho}}_2 = -\frac{K_2\beta S_2 \mathrm{sgn}\left(e_\gamma\right)}{I_z} - \sigma_2\tilde{\rho}_2 \tag{34}$$

$$\dot{\hat{\rho}}_3 = \dot{\tilde{\rho}}_3 = \frac{K_3\delta S_2 \mathrm{sgn}\left(e_\gamma\right)}{I_z} - \sigma_3\tilde{\rho}_3 \tag{35}$$

From Eq. 31 as well as the adaptive laws in Eqs. 33–35, the time derivative of the Lyapunov function in Eq. 29 can be rewritten as follows:

$$\dot{V}_2 = -K_p {S_2}^2 - K_s\left|S_2\right| - \frac{\sigma_1}{K_1}\tilde{\rho}_1^2 - \frac{\sigma_2}{K_2}\tilde{\rho}_2^2 - \frac{\sigma_3}{K_3}\tilde{\rho}_3^2 \tag{36}$$

Hence, $\dot{\hat{V}}_2 < 0$ ensures that the S_2 tracking error and the errors in the estimates of the $\rho_i\,(i=1,3)$ parameters are bounded. Specifically, because the sliding function S_2 is always positive, the proposed control law in Eq. 27 is stable and the tracking error asymptotically converges to zero.

Remark 2: To suppress the chattering phenomenon in the control law in Eq. 27 engendered by disturbances such as variations in driving and road conditions, a modified solution is proposed on the basis of previous study [28]. The solution is obtained by replacing a discontinuous switching function with a saturation function having boundary layer thickness λ_i for the continuous approximation of a signum function as follows:

$$\mathrm{sgn}\left(x_i\right) \approx sat\left(\tfrac{x_i}{\lambda_i}\right) = \begin{cases} \tfrac{x_i}{\lambda_i}, & if \quad \left|\tfrac{x_i}{\lambda_i}\right| < \varepsilon_i, \\ \mathrm{sgn}\left(\tfrac{x_i}{\lambda_i}\right), & \text{otherwise.} \end{cases} \quad (i=1,\ 3) \tag{37}$$

where λ_i and ε_i are low values selected arbitrarily such that the points with high yaw moments are eliminated, and xi is a variable in the signum function.

Therefore, the control law in Eq. 27 becomes

$$\mathrm{sgn}\left(x_i\right) \approx sat\left(\tfrac{x_i}{\lambda_i}\right) = \begin{cases} \tfrac{x_i}{\lambda_i}, & if \quad \left|\tfrac{x_i}{\lambda_i}\right| < \varepsilon_i, \\ \mathrm{sgn}\left(\tfrac{x_i}{\lambda_i}\right), & \text{otherwise.} \end{cases} \quad (i=1,\ 3) \tag{38}$$

In addition, the parameter adaptation laws in Eqs. 33–35 can be updated as follows:

$$\dot{\hat{\rho}}_1 = \dot{\tilde{\rho}}_1 = -\frac{K_1\gamma S_2}{I_z V_x} sat\left(\frac{e_\gamma}{\lambda_1}\right) - \sigma_1\tilde{\rho}_1 \tag{39}$$

$$\dot{\hat{\rho}}_2 = \dot{\tilde{\rho}}_2 = -\frac{K_2 \beta S_2}{I_z} sat\left(\frac{e_\gamma}{\lambda_1}\right) - \sigma_2 \tilde{\rho}_2 \quad (40)$$

$$\dot{\hat{\rho}}_3 = \dot{\tilde{\rho}}_3 = \frac{K_3 \delta S_2}{I_z} sat\left(\frac{e_\gamma}{\lambda_1}\right) - \sigma_3 \tilde{\rho}_3 \quad (41)$$

3.4. Reference variable generators and hydraulic pressure model control system

More details about the definitions of the reference yaw rate, vehicle sideslip angle, and braking pressure, as well as the closed-loop system for hydraulic pressure model control can be found in the previous studies [11, 15].

4. Simulation results

To understand the positive effects of the derived second ASMC algorithm on the control system, the algorithm was compared with the first ASMC algorithm discussed in the previous study [11]. The simulation was performed in a Matlab and Simulink environment and linked to CarSim software for considering different driving maneuvers. References [11, 15] have presented the vehicle configuration parameters, and the parameters of two controllers are listed in Table 2.

The vehicle was assumed to be driven on a road and was considered to have a steering input that changed with the steering wheel angle (Fig. 5).

Each ASMC method was based on the sliding surfaces S_1 and S_2, which are defined in Eqs. 1-2, respectively. The vehicle control performance was verified in terms of variations in road and driving conditions. The driving conditions involved different longitudinal speeds, namely normal speed ($V_x = 100km/h$) and high speed ($V_x = 180km/h$). The road conditions comprised many road surfaces with high friction ($\mu = 0.85$), moderate friction ($\mu = 0.5$), extremely low friction ($\mu = 0.2$), variable friction from a high value of 0.85 to a moderate value of 0.5, and variable friction from a high value of 0.85 to an extremely low value of 0.2.

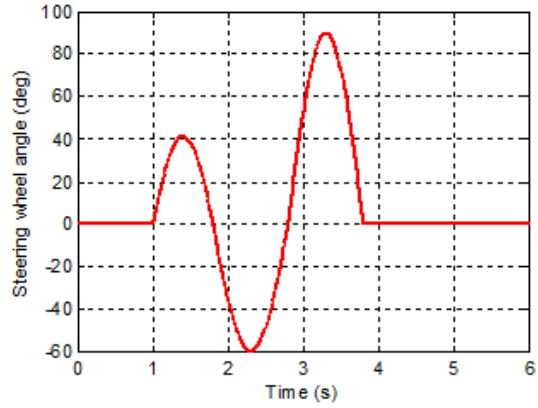

Fig. 5: Structural scheme of a vehicle stability control system.

Tab. 2: Parameters of two controllers.

Symbol	Description	Value
K_p	Constant determining the convergence of tracking error	12
K_s	Constant tuned according to bound of uncertainties	0.5
ξ	Weighting factor	0.01
K_1	Adaptive gain corresponding to estimated parameter ρ_1	0.5
K_2	Adaptive gain corresponding to estimated parameter ρ_2	1.5
K_3	Adaptive gain corresponding to estimated parameter ρ_3	0.9
σ_1	Positive constant corresponding to estimated parameter ρ_1	20
σ_2	Positive constant corresponding to estimated parameter ρ_2	50
σ_3	Positive constant corresponding to estimated parameter ρ_3	30
λ_i	Boundary layer thickness	0.001
ϵ_1	Small positive constant	1

The road and driving conditions were combined to obtain the 10 cases described in Table 3. For each case, the yaw rate and sideslip angle output responses were determined for a vehicle action without control and for a vehicle action with the ASMC algorithms being used. For noncritical road and driving conditions (Case 1, Fig. 6), the yaw rate and sideslip angle responses were stable, even without VSC activation. For all the remaining critical conditions, these responses became unstable for vehicle actions without control. By contrast, depending on the driving maneuver, the yaw

rate and sideslip angle output responses demonstrated the excellent handling behavior of the controllers.

Tab. 3: Comparison based on root mean square errors.

Cases	Vx (km/h)	μ	ASMC 1		ASMC 2	
			$RMSe_\gamma$	$RMSe_\beta$	$RMSe_\gamma$	$RMSe_\beta$
1	100	0.85	0.0159	0.0134	0.0155	0.0134
2	100	0.2	0.0955	0.0633	0.0454	0.0497
3	100	0.85 → 0.2	0.0518	0.0841	0.0470	0.0710
4	100	0.5 → 0.2	0.0604	0.0855	0.0548	0.0592
5	180	0.5 → 0.2	0.2170	0.2503	0.0907	0.0878
6	180	0.85	0.0228	0.0242	0.0207	0.0236
7	180	0.5	0.0182	0.0294	0.0182	0.0294
8	100	0.85 → 0.5	0.0170	0.0212	0.0168	0.0210
9	180	0.85 → 0.5	0.0211	0.0290	0.0187	0.0290
10	180	0.85 → 0.2	0.0874	0.1265	0.0774	0.0915

In Case 1 (Fig. 6), the vehicle was driven at a normal speed on a high-friction surface to determine how the vehicle performance could be improved in noncritical situations. The performance levels of the two controllers in terms of the vehicle yaw rate and sideslip angle responses were difficult to distinguish in this case. Therefore, they were compared by calculating the RMSE values for the yaw rate and sideslip angle, by using the following equation:

$$RMSE = \left(\frac{1}{N} \sum_{k=1}^{N} e(k)^2 \right)^{1/2} \tag{42}$$

where $e(k)$ can be either the yaw rate error (e_γ) or sideslip angle error (e_β), and N is the number of samples.

To facilitate the task of comparing the effects of each of the ASMC algorithms on the vehicle yaw rate and sideslip angle responses, Eq. 42 was used to calculate the RMSE for all the remaining cases; the results are presented in Table 2. Because of the limited number of observations, only the simulation results of the first five cases (Figs. 6-10) are presented in this section;

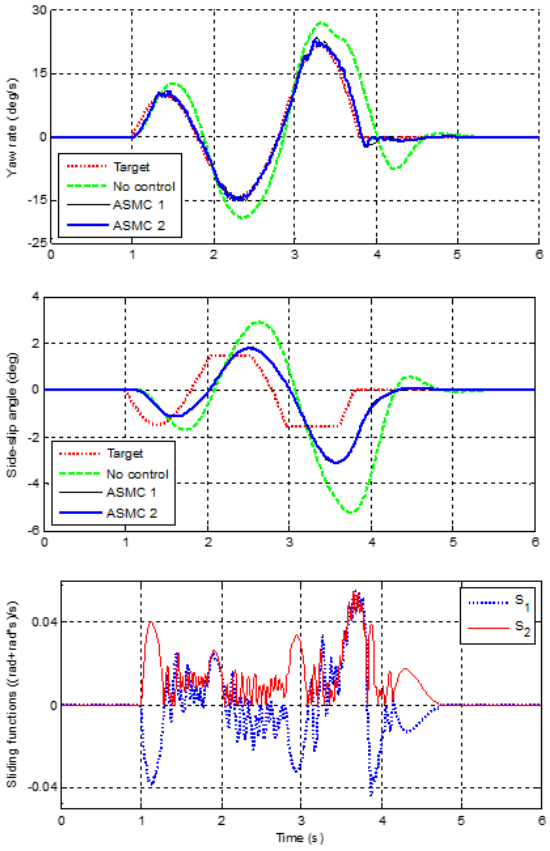

Fig. 6: Simulation results for high friction ($\mu = 0.85$; normal speed: $V_x = 100\ km/h$)

for the remaining five cases, only the calculation results for the yaw rate and sideslip angle RMSE values are discussed.

Fig. 6 shows that the output responses of the yaw rate and sideslip angle were nearly the same for both controllers under the noncritical road and driving conditions. However, the error data in Table 2 for Case 1 show that ASMC 2 is more effective than ASMC 1. In this case, the controllers successfully drove the vehicle according to the steering target; furthermore, the yaw rate response matched its reference almost exactly, and the sideslip angle was within the approximate limit of $\pm 2^0$.

In Case 2 (Fig. 7), the vehicle was driven at a normal speed of 100 km/h on an icy road with an extremely low friction coefficient of 0.2. The objective of this case was to test the stability of the controllers for critical driving ma-

neuvers. The results in Fig. 7 show that both controllers were stable, and the ASMC 2 algorithm converged more rapidly than the ASMC 1 algorithm did. Consequently, as shown in Table 2 (Case 2), the RMSE values for ASMC 2 were considerably lower than those for ASMC 1. The results for ASMC 2 are superior because the sign of S_2 was always positive. Both the yaw rate and sideslip angle errors on the sliding surface were guaranteed to be canceled out. In this critical case, the controllers maintained a stable yaw rate response, and the sideslip angle was within an approximate range of $\pm 6^0$. The next three cases (Figs. 8-10) were considered to test parameter adaptation and the positive effect of the proposed ASMC 2. They were also used to determine whether the performance of the vehicle model improved for some extremely critical driving maneuvers. These cases are discussed in detail as follows.

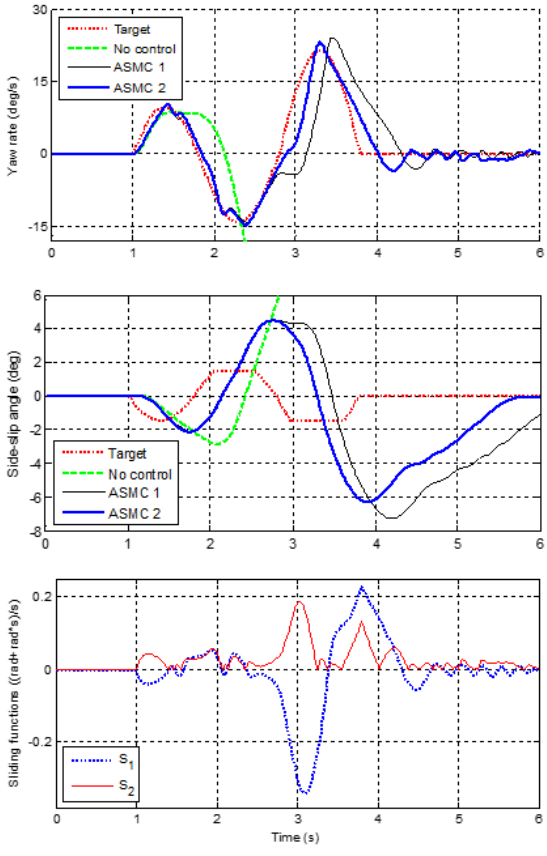

Fig. 7: Simulation results for very low friction ($\mu = 0.2$; normal speed: $V_x = 100\ km/h$).

For Cases 3 and 4 (Figs. 8 and 9), the performance of the controllers was verified by driving a vehicle at a normal speed of 100 km/h on different road surfaces, with the friction coefficients of the road surfaces varying with time from a high value of 0.85 to an extremely low value of 0.2 (Case 3) and from a moderate value of 0.5 to an extremely low value of 0.2 (Case 4). The results in Fig. 8 and the RMSE values in Table 2 (Case 3) indicate that the yaw rate and sideslip angle responses were excellent when the vehicle was driven under normal road driving conditions for the period from 0 to 2.5 s. During this period, these results were the same as those for Case 4 (Fig. 7), for which the RMSE values are shown in Table 2 (Case 4). Subsequently, under road conditions requiring critical driving maneuvers for the period after 2.5 s, the excellent behavior of the controller using ASMC 2 was clear. In particular, the yaw rate tracking response was maintained at a satisfactory level, and the sideslip angle was within an acceptable limit of $\pm 10^0$.

ASMC 1 provided an effective estimation in Case 3 (Fig. 8) but not in Case 4 (Fig. 9). Case 4 involved extremely critical road conditions and driving maneuvers. Therefore, clearly, both the yaw rate and sideslip angle errors were not canceled out in the sliding function S1 when ASMC 1 was used, despite the theoretical demonstration that the algorithm for S_1 asymptotically converged to zero as the time approached infinity. This may be one reason for the failure of ASMC 1 in this case.

For Case 5 (Fig. 10), the vehicle was driven under wet and icy road conditions at a high speed of 180 km/h and friction coefficient varying from a moderate value of 0.5 to an extremely low value of 0.2. The results in Fig. 10 and the RMSE values in Table 2 (Case 5) show that the yaw rate and sideslip angle responses were still favorable when the vehicle was driven under critical road and driving conditions from 0 to 2.5 s. Subsequently, under road conditions requiring extremely critical steering maneuvers for the period after 2.5 s, the controller using ASMC 2 successfully maintained a stable yaw rate response. In particular, the yaw rate tracking response was relatively favorable while the sideslip angle was still within an allowed range of

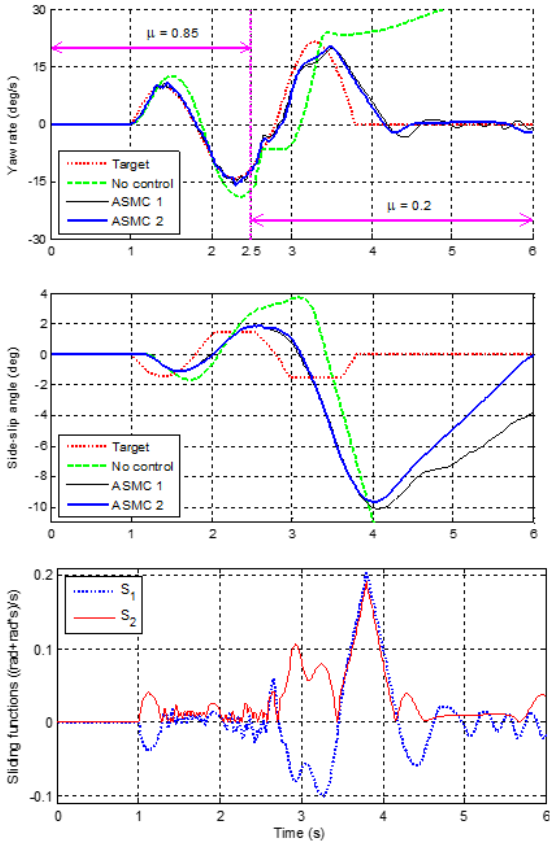

Fig. 8: Simulation results for variable friction ($\mu = 0.85 \rightarrow 0.2$; normal speed: $V_x = 100\ km/h$).

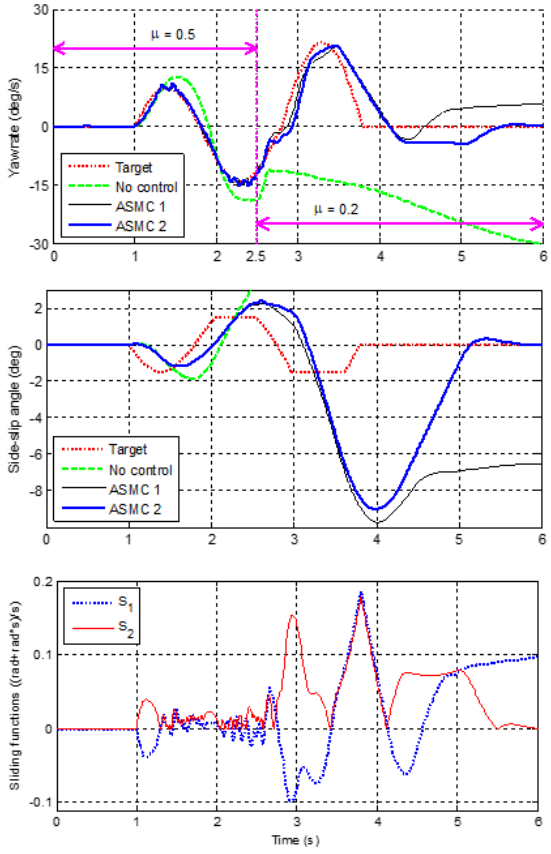

Fig. 9: Simulation results for variable friction ($\mu = 0.5 \rightarrow 0.2$; normal speed: $V_x = 100\ km/h$).

$\pm 12^0$. In this case, ASMC 1 failed as soon as the tire-road friction changed at 2.5 s. To ensure the proposed ASMC2's efficacy in sustaining system stability, simulation time is prolonged 10 seconds as shown in Fig. 11.

The remaining cases (Cases 6–10), for which the RMSE values are shown in Table 2, involved applying ASMC 2 and consistently showed output responses corresponding to the highest performance. Therefore, when ASMC 2 was used, the output responses of the control system were stable in all simulations.

All cases (Figs. 6-10 and Table 2) show that ASMC 2 always yielded more favorable results compared with ASMC 1. Each of the algorithms occasionally exhibited the same effect on the vehicle yaw rate and sideslip angle responses (Case 7 in Table 2). ASMC2 was always effective in Cases 1 (Fig. 6), 2 (Fig. 7), 3 (Fig. 8), and 6–9, and ASMC 1 was also effective in these cases. However, the yaw rate and sideslip angle output responses of ASMC 1 were poorer than those of ASMC 2, with ASMC 1 failing in cases requiring extremely critical driving maneuvers such as Cases 4 (Fig. 9), 5 (Fig. 10), and 10. The reason for the failure is that the sign of the sliding function S_1 of ASMC 1 can be positive or negative. Moreover, the yaw rate and sideslip angle errors were not canceled out simultaneously as the time approached infinity.

In summary, for the 10 cases, the RMSE values shown in Table 2 indicate that ASMC 2 always yielded more favorable results compared with ASMC 1. For instance, the RMSE values were low for ASMC 1 and lower for ASMC 2. The yaw rate response in each case was not smooth because of the effect of the hydraulic pressure model. In practice, the on-and-off frequency of the inlet and outlet valves is 20 ms,

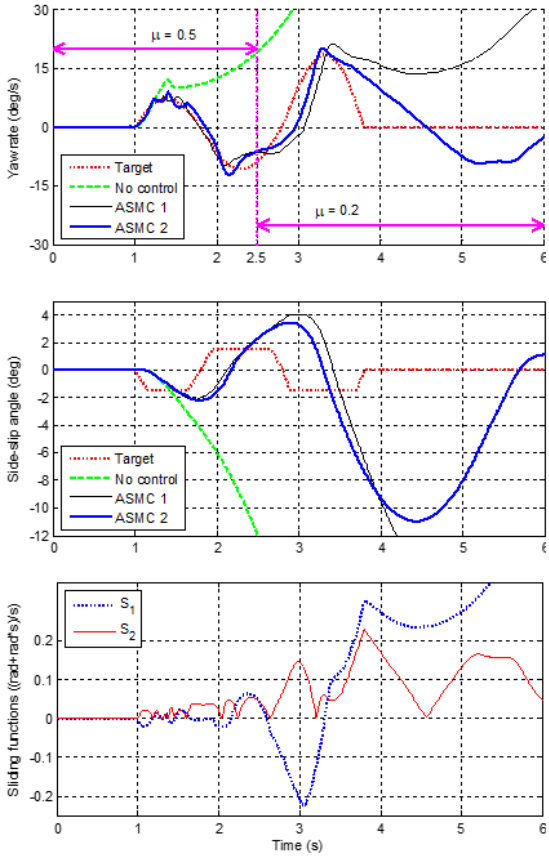

Fig. 10: Simulation results for variable friction ($\mu = 0.5 \rightarrow 0.2$; high speed: $V_x = 180\ km/h$).

whereas the sample time of the reference control signal is 1 ms. In addition, time delay were associated with brake hydraulics and the vehicle response to braking, and they affected the performance of the proposed controller. These delays can be considered uncertainties in the overall system. The results show that the VSC controllers remained robust to disturbances; this is expected because the VSC system stability had been demonstrated using the Lyapunov technique. In particular, the controllers inherited the advantages of sliding mode and adaptive theories. In this study, the Sugeno proportional derivative fuzzy controller was used to control only the hydraulic pressure model for ensuring that the real pressure followed the reference pressure without substantially affecting the output responses of the yaw rate and sideslip angle. In Case 1 (Fig. 6 and Table 2), the yaw rate response almost coincides with the target trajectories.

In the remaining cases (Figs. 7-10 and Table 2), the extremely low friction (icy road) and variable friction (from a dry road to an icy road and from a wet road to an icy road) conditions caused the time responses for the yaw rate and sideslip angle to be slower than those of Case 1. However, the responses were stable. The sideslip angle increased or decreased, depending on the severity of the steering situation. Under driving conditions involving a dry road and normal speed, a wet road and normal speed, and a wet road and high speed, during the initial period from 0 to 2.5 s, the sideslip angle was within the limit of $\pm 2^0$ (Figs. 8- 10). Under driving conditions that became increasingly severe because of the variable frictions and high speed, the sideslip angle gradually outstripped the range of $\pm 2^0$ (Figs. 8-10), but it was still acceptable with an approximate range of $\pm 6^0$, $\pm 10^0$, or $\pm 12^0$.

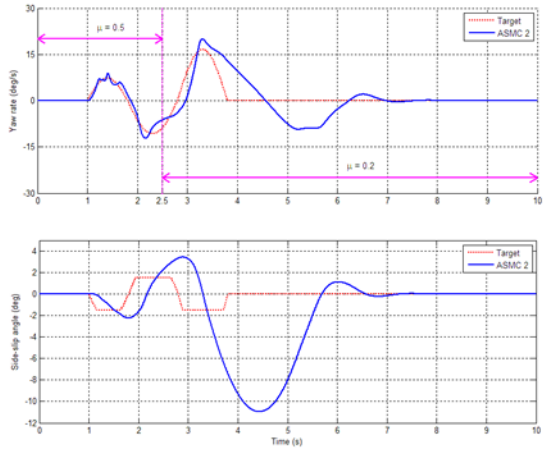

Fig. 11: Simulation results for variable friction ($\mu = 0.5 \rightarrow 0.2$; high speed: $V_x = 180\ km/h$), extending the simulation duration to 10 seconds.

5. Conclusions

This paper describes two ASMC algorithms that can be used for vehicle stability enhancement; the algorithms involve different sliding surfaces. The algorithms were used for testing the tracking performance of each controller and their performance was compared; moreover, verifying the

positive effects of the second ASMC algorithm were determined. The first ASMC algorithm has a drawback: The yaw rate and sideslip angle errors are not guaranteed to cancel out under extremely critical driving conditions. However, the second ASMC algorithm does not have this limitation; in other words, both errors are guaranteed to converge to zero. The simulation results show that a vehicle equipped with the proposed control algorithms can perform critical driving maneuvers to counter external perturbations, namely variations in road and driving conditions.

References

[1] K. Nam, H. Fujimoto, and Y. Hori. Design of an adaptive sliding mode controller for robust yaw stabilisation of in-wheel-motor-driven electric vehicles. *Int. J. Veh. Des.*, 67(1):98–113, 2019.

[2] S. Ghosh, A. Deb, M. Mahala, M. Tanbakuchi, and M. Makowski. Active yaw control of a vehicle using a fuzzy logic algorithm. *SAE Tech. Pap.*, 2012-01-0229, 2012.

[3] M. Canale, L. Fagiano, M. Milanese, , and P. Borodani. Robust vehicle yaw control using an active differential and imc techniques. *Control. Eng. Pract.*, 15:923–941, 2013.

[4] S. Krishna, S. Narayanan, and S.D. Ashok. Fuzzy logic based yaw stability control for active front steering of a vehicle. *J. Mech. Sci. Technol.*, 28(12):5169–5174, 2022.

[5] R. Annamalai, M. Marathe, U.S. Karle, K.P. Venkatesan, C. McCoy, and B. Toth-Antal. Development of vehicle yaw stability controller. *SAE Tech. Pap.*, 2019-26-0086, 2019.

[6] B.C. Chen and F.C. Hsieh. Side-slip angle estimation using extended kalman filter. *Veh. Syst. Dyn.*, 46:353–364, 2011.

[7] B.M. Nguyen, Y. Wang, H. Fujimoto, and Y. Hori. Electric vehicle stability control based on disturbance accommodating kalman filter using gps. *Proc. 2013 IEEE Int. Conf. on Mechatronics (ICM), Vicenza, Italy*, page 382–387, 2017.

[8] A. Nishio, K. Tozu, H. Yamaguchi, K. Asano, and Y. Amano. Development of vehicle stability control system based on vehicle side-slip angle estimation. *SAE Trans.*, 110(6):115–122, 2005.

[9] A.T. Van-Zanten. Bosch esp systems: 5 years of experience. *SAE Trans.*, 109(7):428–436, 2004.

[10] B.L. Boada, M.J.L. Boada, A. Gauchía, E. Olmeda, and V. Diáz. Sideslip angle estimator based on anfis for vehicle handling and stability. *J. Mech. Sci. Technol.*, 29(4):1473–1481, 2018.

[11] A.T. Le and C.K. Chen. Vehicle stability control by using an adaptive sliding-mode algorithm. *Int. J. Veh. Des.*, 72(2):107–131, 2016.

[12] G. Jianhua, C. Liang, Z. Feikun, and Y. Liang. Coordinated control of afs and esp based on fuzzy logic method. *2011 Int. Conf. on Mechatron. Sci. Electr. Eng. Comput. (MEC), Jilin, China*, page 2357–2360, 2011.

[13] M. Choi and S.B. Choi. Model predictive control for vehicle yaw stability with practical concerns. *IEEE Trans. on Veh. Technol.*, 63(8):3539–3548, 2017.

[14] C. Fu, R. Hoseinnezhad, A. Bab-Hadiashar, and R.N. Jazar. Direct yaw moment control for electric and hybrid vehicles with independent motors. *Int. J. Veh. Des.*, 69(1/2/3/4):1–24, 2018.

[15] C.K. Chen, T. Dao, and H.P. Lin. A compensated yaw-moment-based vehicle stability controller. *Int. J. Veh. Des.*, 53(3):220–238, 2010.

[16] P. Raksincharoensak, T. Mizushima, and M. Nagai. Direct yaw moment control system based on driver behaviour recognition. *Veh. Syst. Dyn.*, 46(1):911–921, 2011.

[17] Y.J. Jang and K.H. Nam. The direct yaw-moment control to follow the neutral steering path regardless of velocity. *2014 Int. Power Electron. Conf. Hiroshima, Jpn.*, page 664–670, 2017.

[18] Y. Zhuoping, L .Bo, X. Lu, F. Yuan, and S. Fenmiao. Direct yaw moment control for distributed drive electric vehicle handling performance improvement. *Chin. J. Mech. Eng.*, 29(3):486–497, 2016.

[19] T. Yoshino and H. Nozaki. Effect of direct yaw moment control based on steering angle velocity and camber angle control. *SAE Tech. Pap.*, 2016-01-2386, 2016.

[20] B.C. Chen and C.C. Kuo. Selectric stability control for electric vehicle with four in-wheel motors. *Int. J. Automot. Technol.*, 15:573–580, 2015.

[21] M.T. Emirler, K. Kahraman, and K. SenturM. Lateral stability control of fully electric vehicles. *Int. J. Automot. Technol.*, 16(2):317–328, 2019.

[22] M. Canale, L. Fagiano, A. Ferrara, and C. Vecchio. Vehicle yaw control via second-order sliding-mode technique. *IEEE Trans. on Ind. Electron.*, 55(11):3908–3916, 2010.

[23] S.H. Tamaddoni, S. Taheri, and M. Ahmadian. Optimal preview game theory approach to vehicle stability controller design. *Veh. Syst. Dyn.*, 49(12):1967–1979, 2014.

[24] C.K. Chen and A.T. Le. Vehicle side-slip angle and lateral force estimator based on extended kalman filtering algorithm. *Lect. Notes Electr. Eng.*, 371, 2015.

[25] S. Xuan, G. Meng, L. Jin, and Z. Zheng. Active yaw-moment control based on logic threshold and pid control. *Int. Conf. on Autom. Control. Artif. Intell. Xiamen, China*, page 338–341, 2015.

[26] Anonymity. Carsim reference manual. *Simul. Corp., (2016). Retrieved from http://carsim.com*, 2016.

[27] J.Y. Wong. Theory of ground vehicles. *Third Ed. John Wiley & Sons, USA*, 2001.

[28] J-J.E. Slotine and W. Li. Applied nonlinear control. *In: Sliding control, Englewood Cliffs, Prentice-Hall*, page 267–307, 1991.

About Authors

Anh-Tuan LE received his BS in Mechatronics Engineering from University of Technical Education and MS in Automation Engineering from University of Technology, Ho Chi Minh City, Vietnam in 2006 and 2010, respectively, and PhD in Mechanical and Automatic Engineering from Da-Yeh University, Taiwan, in 2016. He is currently working as a lecturer in Faculty of Electrical and Electronics Engineering, Ton Duc Thang University, Ho Chi Minh City, Vietnam. His current research interests are process control and automation, robot dynamics, vehicle dynamics, vehicle stability control, antilock braking system, traction control system and control applications for vehicles and three-wheeled mobile robots.